Comparing different bulk radiation damage models in TCAD simulations of small-pitch 3D Si sensors

A. Boughedda,[a,b] **M. Lakhdara,**[a] **S. Latreche,**[a] **R. Mendicino,**[c] **and G.-F. Dalla Betta,**[b,d,1]

[a] *Laboratory of Hyper frequencies and Semiconductors, University of Constantine1, Constantine, Algeria*

[b] *Department of Industrial Engineering, University of Trento, Via Sommarive 9, 38123 Trento, Italy*

[c] *Sensors and Devices Center, Fondazione Bruno Kessler, Via Sommarive 18, 38123 Trento, Italy*

[d] *TIFPA INFN, Via Sommarive 14, 38123 Trento, Italy*

E-mail: gianfranco.dallabetta@unitn.it

ABSTRACT: Small-pitch, thin 3D Si sensors have been developed for the ATLAS and CMS experiment upgrades at the High Luminosity LHC. The pixel sizes are 50×50 μm^2 with 1 readout column, and 25×100 μm^2 with 1 or 2 readout columns (1E and 2E). Owing to the small inter-electrode distance, ranging from ~28 μm to ~51 μm in the considered layouts, these devices are expected to be extremely radiation hard. TCAD simulations by Synopsys Sentaurus, incorporating advanced radiation damage models, have been used for the design/optimization of these new 3D pixel sensors. In this study, we have compared the accuracy of different bulk damage models in predicting the signal efficiency of small-pitch 3D sensors irradiated at large fluences and its evolution with the bias voltage at different positions within the 3D cell. Selected simulation results will be reported in comparison to experimental data.

KEYWORDS: Radiation-hard detectors; Radiation damage to detector materials (solid state); Si microstrip and pad detectors; Models and simulations.

[1] Corresponding author.

Contents

1. Introduction

Due to their unique architecture, featuring a short distance between vertical electrodes, 3D pixels are the most radiation-hard silicon sensors [1]. After being used for the first time in the ATLAS Insertable B-Layer [2], they have become natural candidates for the innermost tracking layers of the major detector upgrades at the High Luminosity LHC (HL-LHC). This application has pushed the requirements to the detectors at unprecedented levels in terms of very high hit-rate capabilities and extreme radiation hardness. To this purpose, a new generation of 3D pixels has been developed, having very dense granularity, and reduced active thickness (~150 μm). Two pixel sizes have been considered, compatible with the new read-out chips designed by the RD53 Collaboration [3]: 50×50 μm^2 with 1 readout column, and 25×100 μm^2 with 1 or 2 readout columns (1E and 2E). Besides maintaining the occupancy at ~% level and improving the spatial resolution, these small-pitch 3D geometries feature a reduced inter-electrode distance, ranging from ~28 μm to ~51 μm in the considered layouts, thus enhancing the radiation hardness [4].

Since 2013, in the framework of an R&D program funded by INFN, several batches of small-pitch 3D sensors aimed at the ATLAS and CMS upgrades were fabricated at FBK using a single-sided technology on Si-Si Direct Wafer Bonded 6" substrates [5-7]. Pixel sensors compatible with different read-out chips (ATLAS FEI4, CMS PSI46dig, and RD53A) were tested under particle beams before and after irradiation, showing a very high hit efficiency of ~97% after an irradiation fluence of 1×10^{16} n_{eq} cm^{-2} [8-10]. Further tests aimed at assessing the performance up to the ~2× larger fluences of interest for the HL-LHC experiments are under way. The radiation hardness of FBK small-pitch 3D sensors irradiated up to extremely large fluences has so far been measured on test structures: the results of position resolved laser tests performed on 3D diodes of various geometries after neutron irradiation up to 3.5×10^{16} n_{eq} cm^{-2} are discussed in [11], showing very high signal efficiency, also boosted by charge multiplication effects.

In this paper, extending our preliminary studies [12,13], we compare the accuracy of two advanced bulk damage models in predicting the signal efficiency of small-pitch 3D sensors irradiated at different fluences in the range of interest for HL-LHC, and its evolution with the bias voltage at different positions within the 3D cell. Selected simulation results will be reported in comparison to experimental data from [11].

2. Simulation approach

TCAD simulations were performed by Synopsys Sentaurus, aimed at evaluating the signal efficiency (SE), that is defined as the ratio of the charge signal amplitude after irradiation and

before irradiation. To this purpose, keeping into account that the electric field in the vertical direction is uniform for most of the sensor depth, a simplified quasi-2D domain was used, consisting of a sensor slice, 1-µm thick, taken at half the depth of the structures. Simulations also exploit the inherent 3D pixel symmetry to minimize the number of grid points and therefore the simulation time. The simulated structures consist of a 1/4 of a pixel in case of the 50×50-1E and 25×100-1E pixels, and of 1/8 of a pixel in case of the 25×100-2E pixel (see Figure 1).

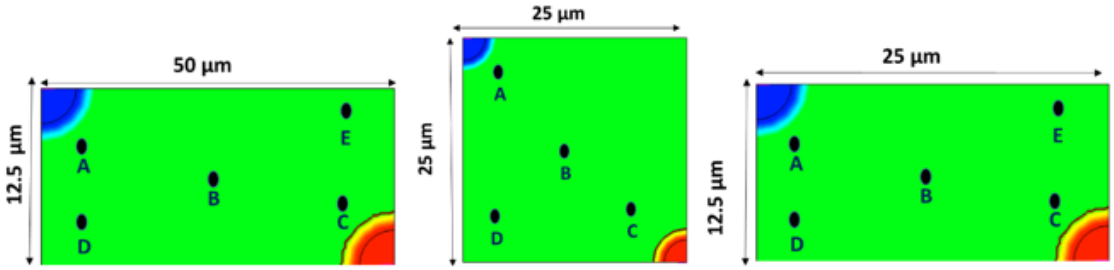

(a) **(b)** **(c)**

Figure 1. Simulation domains are horizontal slices taken at half the depth of different 3D pixel sensors and exploiting the symmetry in the 3D cells: a) 25×100-1E, b) 50×50-1E, and c) 25×100-2E. The readout column is shown in red at the bottom right corner, the bias column in blue at the top left corner. The simulated hit points are also shown, and their coordinates are detailed in Table 1.

Table 1. Coordinates of different hit points within the simulation domains of the three pixel structures.

Structures	25×100-1E		50×50-1E		25×100-2E	
Hit point	X (µm)	Y (µm)	X (µm)	Y (µm)	X (µm)	Y (µm)
A	2	4	5.6	5.6	5.9	4
B	25	6.25	12.5	12.5	12.5	6.25
C	48	8.5	19.1	19.1	19.1	8
D	2	10.5	5.6	19.1	5.9	8
E	48	2	-	-	19.1	4

Simulations use typical models (e.g., effective intrinsic density, doping dependent Shockley-Read-Hall generation/recombination and mobility, high field saturation, etc.) and default values for most parameters but the minority carrier lifetimes, for which values of ~ms were chosen, typical of FBK technology. Impact ionization effects are incorporated according to the avalanche model by Van Ovestraeten/De Man. The "Heavy Ion" model was used to release charge packets at different hit positions within the simulation domain with a uniform distribution along the vertical axis and a Gaussian distribution across the horizontal plane.

Radiation damage effects in the silicon bulk are simulated using two deep-level trap models, i.e., the Perugia model [14] and the CERN model [15]. Both models are tuned for p-type silicon and use two acceptor trap levels and one donor trap level, with different values of the relevant parameters. The Perugia model has been validated at different temperatures (here we use room temperature) up to a fluence of 2.2×10^{16} n_{eq} cm^{-2}. The CERN model has been validated for a temperature range from -38.1 ºC to -31.1 ºC (here we use -37.9 ºC) up to a radiation fluence of 8×10^{15} n_{eq} cm^{-2}, but is here used beyond this limit.

Simulations start with a quasi-static analysis to save the different bias voltage conditions, that are later fed as initial conditions for the transient analysis. The output of transient simulations

provides current pulses at the readout electrode as a function of time. The leakage current is subtracted from the current pulse and a numerical integration in the time domain is performed over 20 ns (compatible with LHC bunch-crossing), yielding the charge signal.

3. Results

For the sake of conciseness, the analysis will be mainly focused on the 50×50-1E structure, but more general considerations will be drawn from the reported results and comparisons.

The signal efficiency as a function of reverse voltage at different hit points, simulated with the Perugia and the CERN model for the 50×50-1E pixel irradiated at 1×10^{16} n_{eq} cm^{-2} and 2×10^{16} n_{eq} cm^{-2} is shown in Figures 2 and 3, respectively. In all cases, data show different trends for different hit points, as expected. However, for all hit points the SE reaches high values as voltage is increased, with a smoother rise for the CERN model, and also exceeding 100% at high voltage due to charge multiplication effects.

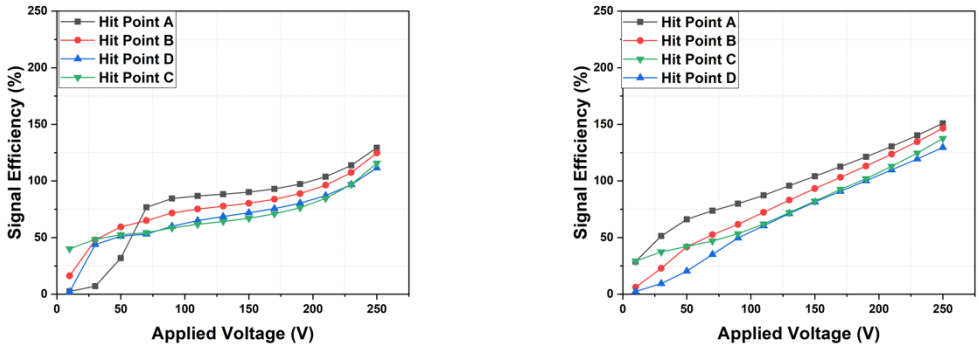

Figure 2. Simulated signal efficiency vs reverse voltage at different hit points for the 50×50-1E pixel irradiated at 1×10^{16} n_{eq} cm^{-2}: (left) Perugia model; (right) CERN model.

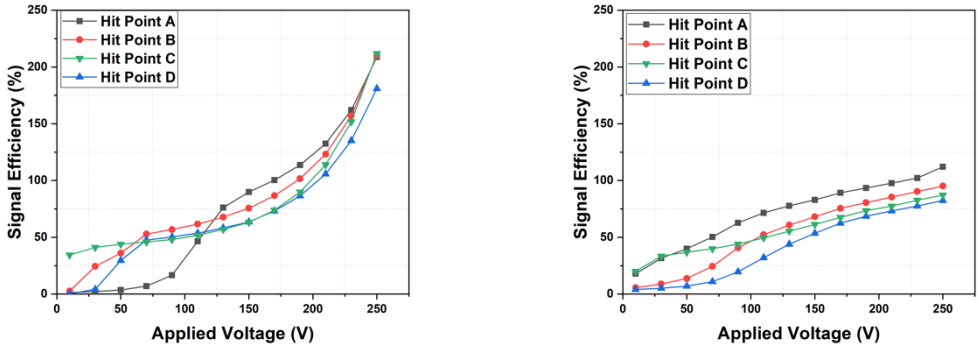

Figure 3. Simulated signal efficiency vs reverse voltage at different hit points for the 50×50-1E pixel irradiated at 2×10^{16} n_{eq} cm^{-2}: (left) Perugia model; (right) CERN model.

To gain more insight into the outcome from the two models, Figure 4 compares the simulated SE at hit points A (close to the bias column) and C (close to the readout column) to the

experimental values measured on the same points from [11] for the 50×50-1E pixel irradiated at 2×10^{16} n_{eq} cm^{-2}. For hit point A, simulations using the CERN model slightly overestimate the measured SE, but the overall trend with voltage is similar. On the contrary, for the Perugia model, the SE is initially very low, and then increases abruptly as the voltage is increased, finally diverging due to charge multiplication effects. For hit point C, simulations using the CERN model slightly underestimate the measured SE but show again a similar trend with voltage. On the contrary, for the Perugia model, the simulated SE initially increases more rapidly than the experimental one, and then reaches comparable values in the intermediate voltage range, before diverging due to charge multiplication effects.

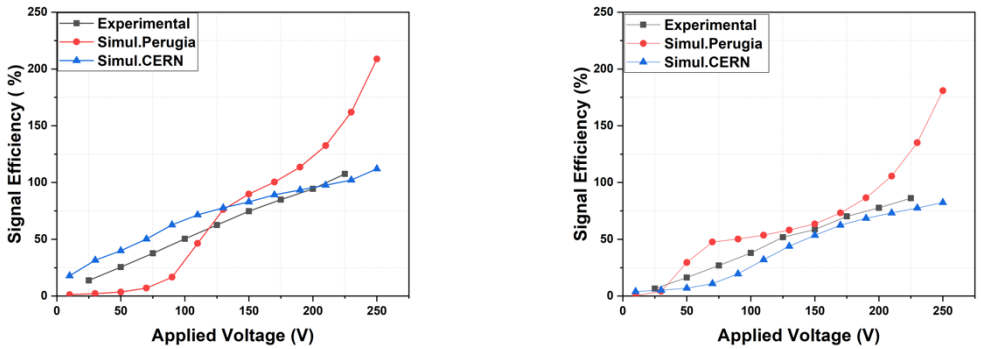

Figure 4. Simulated and experimental signal efficiency vs reverse voltage at different hit points for the 50×50-1E pixel irradiated at 2×10^{16} n_{eq} cm^{-2}: (left) hit point A; (right) hit point C.

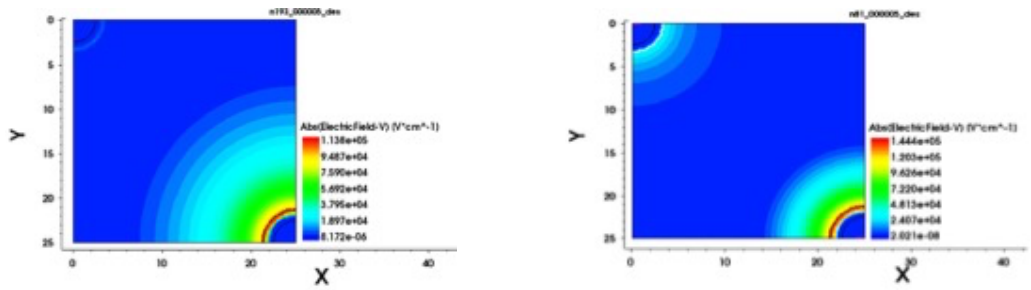

Figure 5. Two-dimensional maps of the electric field at 50 V reverse bias for the 50×50-1E pixel irradiated at 2×10^{16} n_{eq} cm^{-2}: (left) Perugia model; (right) CERN model.

Keeping into account the Ramo's theorem, and the fact that the weighting field in 3D sensors exhibits peaks close to both types of electrodes [16], the different trends in the simulated SE can be explained by the different electric field distributions obtained with the two models, that are shown in Figures 5 and 6 at reverse bias of 50 V and 200 V, respectively. At 50 V, the Perugia model predicts a wider depletion region spreading from the readout column, with no sign of an electric field peak at the bias column: this justifies the low SE at hit point A and the relatively high SE at hit point C, mainly due to the electron contribution to the signal. On the contrary, the CERN model shows a double peak of electric field at the two columns, with a narrower extension of the depletion region at the readout column, compatible with results observed at both points A

and C, with a more balanced contribution to the signal from both electrons and holes. At 200 V, the electric field distributions are more similar, and a double peak of electric field is also predicted by the Perugia model, albeit less pronounced than for the CERN model; moreover, the electric field intensity at the readout column is higher with the Perugia model, that can explain the greater impact of charge multiplication on the simulated SE.

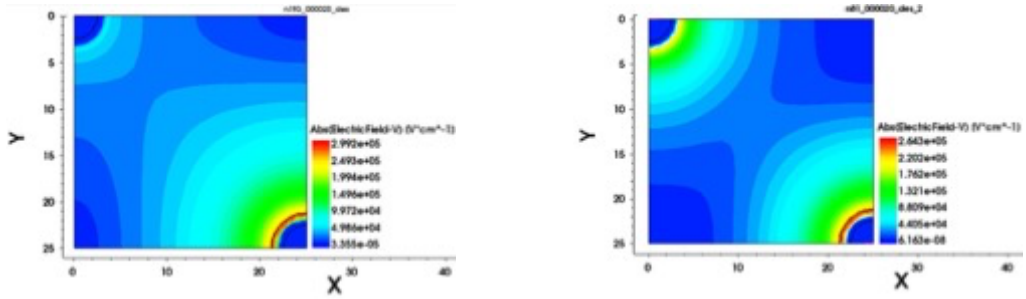

Figure 6. Two-dimensional maps of the electric field at 200 V reverse bias for the 50×50-1E pixel irradiated at 2×10^{16} n_{eq} cm^{-2}: (left) Perugia model; (right) CERN model.

Figures 7 and 8 compare the simulated SE to the experimental values from [11] for all the pixel geometries irradiated at 1×10^{16} n_{eq} cm^{-2} and 2×10^{16} n_{eq} cm^{-2}, respectively. The experimental data represent the average of the values measured along the diagonal connecting the centers of bias and readout columns, excluding the regions covered by metal, whereas the error bars are the standard deviations. The simulated values represent the average between hit points A, B, and C. At 1×10^{16} n_{eq} cm^{-2} the agreement between simulations and measurements is good enough for the 50×50-1E structure, whereas simulations underestimate the signal efficiency for the 25×100-2E structure (note that experimental data are not available at this fluence for the 25×100-1E geometry). At 2×10^{16} n_{eq} cm^{-2} the agreement between simulations and measurements is better for both Perugia and CERN models for all geometries, at least up to ~150 V. At larger voltage the agreement is still acceptable with the CERN model, whereas larger deviations are observed with the Perugia model.

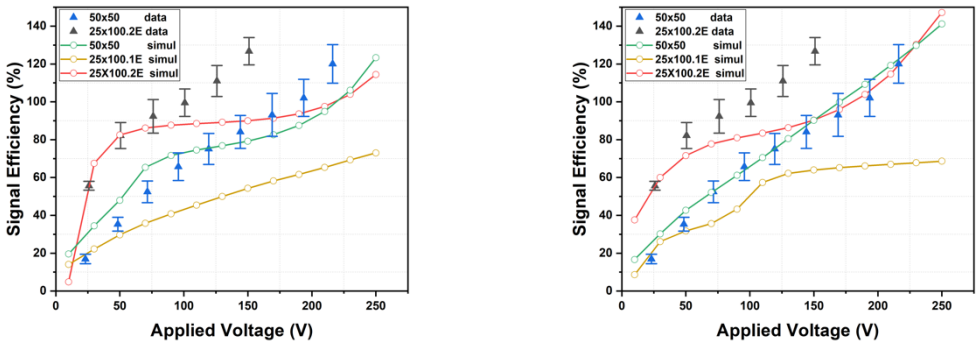

Figure 7. Average signal efficiency vs reverse voltage for all pixel geometries irradiated at 1×10^{16} n_{eq} cm^{-2}: (left) Perugia model; (right) CERN model. Experimental data are not available for the 25×100-1E geometry.

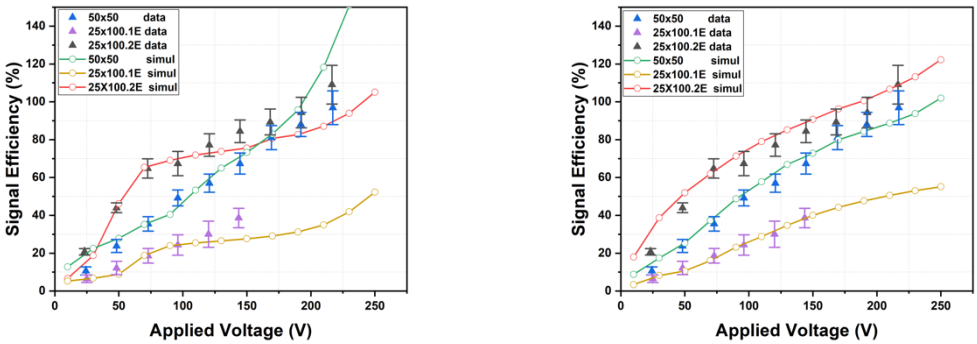

Figure 8. Average signal efficiency vs reverse voltage for all pixel geometries irradiated at 2×10^{16} n_{eq} cm^{-2}: (left) Perugia model; (right) CERN model.

In general, the larger discrepancies between simulations and measurements appear at large voltage, when charge multiplication effects play a major role. In this respect, it should be noted that both the junction between the readout columns and the p-spray implant close to the front-side surface, and the readout column tips can experience high electric field peaks [17], so the simplified quasi-2D domain here used is not entirely adequate. Moreover, simulations are performed at the temperatures for which the radiation damage models were validated, that differ from the temperature at which the measurements were performed (-10 ºC [11]), so that the impact ionization coefficients can be affected.

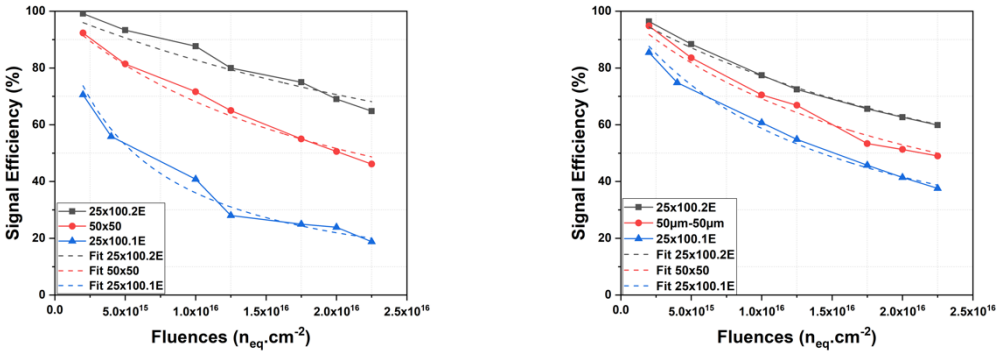

Figure 9. Average signal efficiency vs fluence for all pixel geometries with fits according to the geometrical model of [4]: (left) Perugia model; (right) CERN model.

Figure 9 shows the simulated SE at ~100 V (i.e., below the onset of charge multiplication) as a function of the fluence within an extended range from 2×10^{15} n_{eq} cm^{-2} to 2.25×10^{16} n_{eq} cm^{-2} for the three considered structures. As expected from geometrical consideration, the SE values decrease as the inter-electrode distance is increased. The fitting curves of simulated data according to the theoretical model of Eqn.1 are also shown in Fig. 9 [4]:

$$SE = \frac{1}{1+K_c\varphi} = \frac{1}{1+0.6\,L\,K_L\varphi} \qquad (1)$$

where K_c and K_L are damage parameters, L is the inter-electrode distance, and φ is the fluence. The values of L and the best-fit values of K_c and K_L are reported in Table 2.

Table 2. Best-fit values of damage parameters K_c and K_L for the different pixel structures.

	Model	Perugia		CERN	
Structures	L (μm)	K_c (10^{-16} cm^2)	K_L (10^{-14} cm)	K_c (10^{-16} cm^2)	K_L (10^{-14} cm)
25×100-1E	51.5	1.78 ± 0.13	5.75 ± 0.43	0.70 ± 0.02	2.27 ± 0.07
50×50-1E	35.4	0.47 ± 0.02	2.20 ± 0.11	0.45 ± 0.02	2.11 ± 0.08
25×100-2E	28.0	0.21 ± 0.02	1.24 ± 0.13	0.29 ± 0.01	1.76 ± 0.04

It can be seen from Figure 9 and Table 2 that the two models yield comparable values for the 50×50-1E structure, whereas more significant differences are found for the other geometries, especially for the 25×100-1E. In this respect, the spread in the values of K_L (that should ideally be a constant in case charge carriers reach saturation velocity [4]) is limited for the CERN model, whereas it is much wider for the Perugia model, which seems to overestimate the dependence of radiation hardness on the inter-electrode distance.

4. Conclusion

In this paper we have reported on a TCAD simulation study relevant to the signal efficiency of small-pitch 3D sensors of different geometries fabricated at FBK and irradiated at large fluences up to the maximum value foreseen at the innermost pixel layers at HL-LHC (2×10^{16} n_{eq} cm^{-2}). Simulations have been performed using a simplified quasi-2D domain, corresponding to a horizontal slice, 1-μm thick, taken at half the depth of the structures. Results based on two bulk damage models were analyzed, in comparison with experimental data from 3D diodes measured with a position resolved laser system. Despite both models were validated against data from planar sensors, they predict signal efficiency values and charge multiplication effects at high voltage that are compatible with the experimental observations. Due to the different distributions of the electric field, and particularly to the presence/intensity of the double peak, the two models yield a different evolution of the signal efficiency with bias voltage at different hit points, that is found in better agreement with measurements in case of the CERN model. For both models, simulations show the largest deviations from measurements at high voltage, beyond the onset of charge multiplication. To better investigate this aspect, we plan to further extend this study using a full 3D simulation domain, thus including those regions that can play a critical role for high field effects.

Acknowledgments

This project has received funding from the European Union's Horizon 2020 Research and Innovation programme under Grant Agreement no. 654168. This work was also supported by the Autonomous Province of Trento, the Italian National Institute for Nuclear Physics (INFN) and the Algerian Directorate General for Scientific Research and Technological Development (DGRSDT).

References

[1] C. Da Via, G.-F. Dalla Betta, and S. Parker, *Radiation sensors with three-dimensional electrodes,* CRC Press, Boca Raton, U.S.A., 2019.

[2] C. Da Via et al., *3D Silicon Sensors: Design, Large Area Production and Quality Assurance for the ATLAS IBL Pixel Detector Upgrade*, Nucl. Instrum. Meth. A **694** (2012) 321.

[3] M. Garcia-Sciveres, J. Christiansen, *Development of pixel readout integrated circuits for extreme rate and radiation*, CERN-LHCC-2013-002, LHCC-I-024. http://rd53.web.cern.ch/RD53

[4] C. Da Vià, S.J. Watts, *The geometrical dependence of radiation hardness in planar and 3D silicon detectors*, Nucl. Instrum. Meth. A **603** (2009) 319.

[5] G.-F. Dalla Betta et al, *Development of a new generation of 3D pixel sensors for HL-LHC*, Nucl. Instrum. Meth. A **824** (2016) 386.

[6] D M S Sultan et al., *First production of new thin 3D sensors for HL-LHC at FBK*, JINST **12** (2017) C01022.

[7] M. Boscardin et al., *Advances in 3D Sensor Technology by Using Stepper Lithography,* Frontiers in Physics - Radiation Detection and Imaging **8** (2021) 625275.

[8] H. Oide et al., *INFN-FBK developments of 3D sensors for High-Luminosity LHC*, Nucl. Instrum. Meth. A **924** (2019) 73.

[9] M. Boscardin et al., *Performance of new radiation-tolerant thin planar and 3D columnar n^+ on p silicon pixel sensors up to a maximum fluence of ~5×10^{15} n_{eq}/cm^2*, Nucl. Instrum. Meth. A **953** (2020) 163222.

[10] S. Terzo et al., *Novel 3D pixel sensors for the upgrade of the ATLAS Inner Tracker,* Frontiers in Physics - Radiation Detection and Imaging **8** (2021) 624668.

[11] R. Mendicino et al., *Characterization of FBK small-pitch 3D diodes after neutron irradiation up to 3.5×10^{16} n_{eq} cm^{-2}*, JINST **14** (2019) C01005.

[12] G.-F. Dalla Betta et al., *Development of new 3D pixel sensors for phase 2 upgrades at LHC*, IEEE NSS/MIC Conference Record, San Diego, USA (2015) N3C3-5.

[13] A. Boughedda et al., *TCAD simulation of small-pitch 3D sensors for pixel detector upgrades at High Luminosity LHC*, J. Phys.: Conf. Ser. **1766** (2021) 012014.

[14] F. Moscatelli et al., *Combined Bulk and Surface Radiation Damage Effects at Very High Fluences in Silicon Detectors: Measurements and TCAD Simulations,* IEEE Trans. Nucl. Sci. **63** (2016) 2716.

[15] Å. Folkestad et al., *Development of a silicon bulk radiation damage model for Sentaurus TCAD,* Nucl. Instrum. Meth. A **874** (2017) 94.

[16] M. Koehler et al., *Comparative measurements of highly irradiated n-in-p and p-in-n 3D silicon strip detectors*, Nucl. Instrum. Meth. A **659** (2011) 272.

[17] G.-F. Dalla Betta et al, *Electrical characterization of FBK small-pitch 3D sensors after γ-ray, neutron and proton irradiations,* JINST **12** (2017) C11028.